Resonant Ultrasound Microscopy with Isolated Langasite Oscillator for Quantitative Evaluation of Local Elastic Constant

Hirotsugu OGI, Jiayong TIAN, Toyokazu TADA and Masahiko HIRAO

Graduate School of Engineering Science, Osaka University, 1-3 Machikaneyama, Toyonaka, Osaka 560-8531, Japan

A resonant-ultrasound-microscopy method has been developed for measuring the local Young's modulus of a material. This method detects the effective Young's modulus through the resonance frequency of a langasite ($La_3Ga_5SiO_{14}$) oscillator touching the specimen. Because the vibration of the oscillator is induced and detected with a solenoid coil in noncontacting, wireless, and electrodeless way, it is affected only by its contact with the specimen, achieving an absolute measurement. Elastic-constant mapping was performed on cross sections of a duplex stainless steel and a NbTi/Cu superconducting wire. Analysis with the static contact stiffness predicts the frequency change smaller than that measured, and the necessity of considering the dynamic contact stiffness is discussed.

KEYWORDS: elastic constants, microscopy, langasite, noncontact measurement, resonance ultrasound spectroscopy

1. Introduction

Measurement of the elastic constants of solids in micro- and nanoscale regions has been an important issue because of three requirements: (i) The elastic constants are needed to calculate residual stresses in multiphase composites caused by lattice misfit and different thermal-expansion coefficients among different elements. (ii) They are indispensable for the calculation of the strain-energy distribution to find the minimum of the free energy to estimate possible lattice structures. (iii) They can be used for evaluating defects because defects such as vacancies, dislocations, and microcrackings affect elastic constants in a local area and we can evaluate the material's deterioration by measuring the local elastic constants.

Elastic-stiffness mapping has been achieved by ultrasound-atomic-force microscopy (UAFM).[1–6] It utilizes the vibration of an atomic-force-microscopy (AFM) cantilever contacting the material at the free end through a needle tip. This technique yields an image reflecting the material's elastic property in a nanoscale region from the change in the resonance frequency of the cantilever. The UAFM method has made it possible to quantitatively evaluate the effective Young's modulus of a solid after a calibration measurement. However, this method may include difficulties for achieving an absolute determination of a material's stiffness because contact to the vibrating cantilever occurs not only with the specimen but also with the attached piezoelectric oscillator and the fixed end. To calculate the resonance frequencies of such a composite system, we need exact values of the dimensions, elastic constants, and mass densities of all the participating components. Rigidity at the fixed end will also affect the measurements because the maximum bending and torsional stresses appear on the surface at the fixed end. To overcome these problems, we must isolate the vibration of the oscillator so that it makes only one-point contact with the specimen.

Here, we propose a resonant-ultrasound microscopy technique for measuring the local elastic constants of materials. This method adopts a monocrystal langasite ($La_3Ga_5SiO_{14}$) as an oscillator. Langasite belongs to the group of materials with 32-point-group symmetry (trigonal) that show six independent elastic constants C_{ijkl}, two piezoelectric coefficients e_{ijk}, and two dielectric coefficients ϵ_{ij}.[7,8] Because the normalized temperature derivatives of C_{ijkl} are small, of the order of 10^{-5}-10^{-6}, the resonance frequencies of a langasite oscillator are insensitive to temperature change. Also, langasite shows good piezoelectricity, which allows one to oscillate the crystal in a noncontacting manner using a dynamic electric field.[8] Neither wires nor electrodes are needed. Thus, the contact to the crystal is made only with the specimen and any other acoustical contacts can be eliminated. This technique, therefore, negligibly includes the measurement errors associated with contact coupling and ambiguous boundary conditions. Measuring the resonance frequency and scanning the object surface then provide us with an image of elastic-stiffness distribution. Further advantages include the high accuracy of the vibrational analysis because of the simple vibrational system. We show elastic-constant images for a duplex stainless steel and a superconducting wire. Our measurements indicate the necessity of the consideration of the dynamic contact stiffness in this field of study.

2. Isolation of Langasite Crystal

Figure 1 shows the measurement setup.[9] An oriented rectangular parallelepiped langasite is located inside the solenoid coil. The principal lengths of the crystal along the x_1, x_2, and x_3 axes are 4.954, 5.769, and 4.016 mm, respectively. We took x_1 and x_3 axes as the two-fold and three-fold axes, respectively. A surface normal to the x_1 axis contacts a specimen surface through a tungsten-carbide bearing ball attached to the center of the bottom surface of the crystal. When a sinusoidal tone-burst current is applied to the solenoid coil, an oscillating quasi-static electric field arises along the axial direction of the coil that vibrates the crystal via the converse piezoelectric effect. After the excitation, the same coil receives the vibration through the piezoelectric effect.[8] The received signals enter a superheterodyne spectrometer and the amplitude component with the same frequency as the driving current is extracted.[10–12] A frequency scan provides the resonance spectrum. Fitting a Lorentzian function yields the resonance frequency.

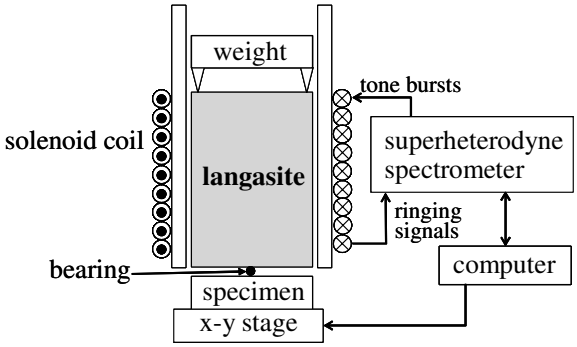

Fig. 1. Measurement setup of resonant-ultrasound microscopy with rectangular-parallelepiped langasite oscillator.

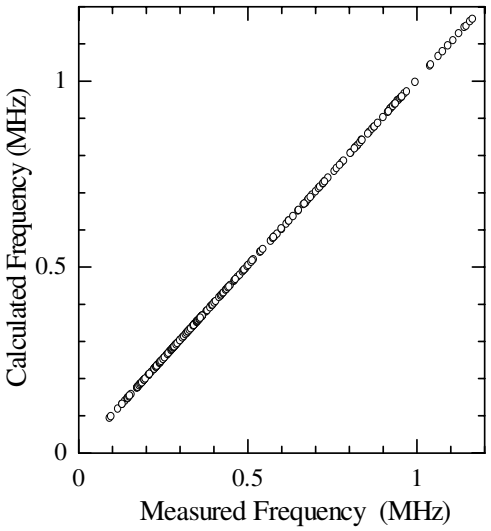

Fig. 2. Measured and calculated resonance frequencies of rectangular-parallelepiped langasite oscillators. Results for five oscillators with different volumes are shown together. The rms difference between them is 0.065%.

There are numerous vibration modes and we select a mode that shows a center antinode spot on the bottom surface and a nodal line on the top surface of the oscillator as shown in the following section in detail. A biasing force F_0 is applied to support the crystal and to make the sensitivity to the contact stiffness higher through three pins touching the vibrational nodes on the top surface. Thus, the acoustic coupling only occurs at the specimen surface and the vibration of the crystal is isolated from any other contacts, realizing high sensitivity and reproducibility of the measurement.

3. Analysis of Vibration by Rayleigh-Ritz Method

There are four groups of the natural vibrations of an oriented rectangular-parallelepiped crystal with 32-point-group symmetry. They are denoted as A_g, B_g, A_u, and B_u, according to the deformation symmetry as tabulated by Ohno.[13] Resonance frequencies and vibration modes are calculated using Lagrangian minimization and the Rayleigh-Ritz method.[13–15] When there is contact on the surface of the crystal, resonance frequencies change from those under free vibration. According to the Hertzian-contact model, the contact between the bearing ball and specimen can be regarded as an elastic spring. The equivalent static spring constant for an isotropic material is given by[6,16]

$$k = \sqrt[3]{6E^{*2}RF_0}. \tag{1}$$

Here, E^* denotes the effective Young's modulus of the specimen:

$$\frac{1}{E^*} = \frac{1-\nu_1^2}{E_1} + \frac{1-\nu_2^2}{E_2}. \tag{2}$$

E and ν denote Young's modulus and Poisson's ratio. Subscripts 1 and 2 denote the bearing ball and specimen, respectively. For the bearing ball, E_1=630 GPa and ν_1=0.2. The Lagrangian of the vibration system can be expressed by

$$L = \frac{1}{2}\int_V \left(S_{ij}C_{ijkl}S_{kl} - \frac{\partial\phi}{\partial x_m}\epsilon_{mn}\frac{\partial\phi}{\partial x_n} + 2\frac{\partial\phi}{\partial x_m}e_{mkl}S_{kl} - \rho\omega^2 u_i^2 \right) \mathrm{d}V - \frac{1}{2}m\omega^2\tilde{u}^2 + \frac{1}{2}k\tilde{u}^2. \tag{3}$$

Here, u_i and S_{ij} denote displacements and the strain tensor, respectively. ϕ, ρ, and ω are the electric potential, the mass density of langasite, and the angular resonance frequency of the system, respectively. $\tilde{u}$ denotes the out-of-plane displacement of the oscillator at the contact point. m is the mass of the bearing ball; attachment of the bearing ball is equivalent to an addition of a point mass on the oscillator surface. Thus, the first term on the right-hand side of eq. (3) denotes the Lagrangian of the langasite crystal consisting of the elastic-strain energy, the coupling energy, the electric energy, and the kinetic energy. The second term expresses the kinetic energy of the bearing ball, and the last term denotes the elastic energy caused by the contact stiffness. Because the displacements and electric potential are analytically unavailable, we approximated them with linear combinations of the basis functions consisting of normalized Legendre polynomials (Rayleigh-Ritz approach):

$$u_i(x_1,x_2,x_3) = \sum_k a_k^i \Psi_k^i(x_1,x_2,x_3), \tag{4}$$

$$\phi(x_1,x_2,x_3) = \sum_k a_k^\phi \Psi_k^\phi(x_1,x_2,x_3). \tag{5}$$

Here,

$$\Psi_k(x_1,x_2,x_3) = \frac{1}{\sqrt{L_1L_2L_3}}\sqrt{\frac{2l+1}{2}}\sqrt{\frac{2m+1}{2}} \times$$

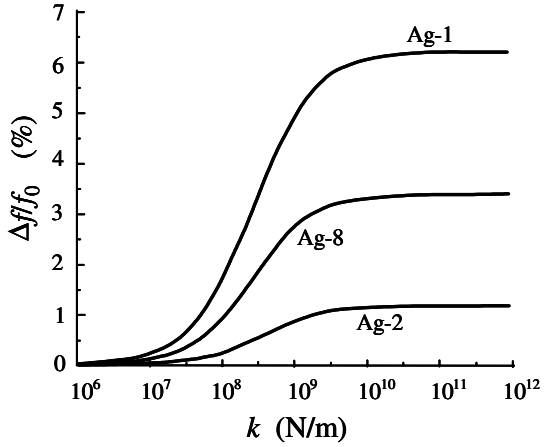

Fig. 3. Dependences of resonance frequencies in A_g vibration group on static contact stiffness. f_0 denotes frequencies under free vibrations.

$$\sqrt{\frac{2n+1}{2}} P_l\left(\frac{x_1}{L_1}\right) P_m\left(\frac{x_2}{L_2}\right) P_n\left(\frac{x_3}{L_3}\right). \quad (6)$$

L_i denotes the edge length along the x_i axis of the rectangular-parallelepiped crystal. The stationary point of the Lagrangian ($\delta L = 0$) yields the resonance frequencies of the system and the corresponding sets of expansion coefficients a_k^i through the solving of an eigenvalue problem. The maximum order of the Legendre polynomials used in the calculation was twelve and the total number of basis functions was 455 for each vibration group. Figure 2 shows a comparison of the calculated resonance frequencies with measured values for five langasite crystals with different volumes ranging between 44.6 and 1442 mm^3 when there is no contact. They show excellent agreement; their rms difference was 0.065%. Thus, the resonance frequencies are accurately calculated because of the use of a simple vibrational system utilizing the noncontact excitation and detection of vibration. This is a great advantage because the analysis only requires the crystal's dimensions, and its elastic, piezoelectric, and dielectric coefficients, and the mass of the bearing ball, which are all unambiguously known.

We used the A_g-1 mode (fundamental mode of breathing vibration) because it shows high sensitivity to the contact stiffness. Figure 3 shows the relationship between the resonance-frequency shift and the contact stiffness. The A_g-1 mode shows the highest sensitivity to the contact stiffness because it has a large out-of-plane amplitude at the contact point. Also, this mode is ideal because it provides an antinode point at the center of the bottom surface for the out-of-plane displacement and nodal lines on the top surface for the in-plane displacements, as shown in Fig. 4. Thus, this mode is sensitive to the normal Young's modulus. We applied a biasing force on the nodal lines through three needles so that these contacts did not affect the vibration.

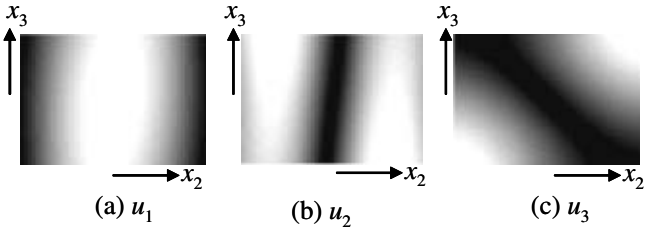

Fig. 4. Distributions of displacements on the bottom surface of the langasite crystal for A_g-1 mode. (a), (b), and (c) are distributions for out-of-plane displacement and two in-plane displacements, respectively.

4. Microscopy

We scanned the cross sections of two materials by measuring the resonance frequency every 5 μm. We used a weight to cause a constant biasing force (F_0=0.13 N). The measurements were performed in a vacuum (∼1 Pa) to avoid acoustic noise. The first material tested was a duplex stainless steel (JIS-SCS13A). It consists of a ferrite phase (α phase) with 17.2% volume fraction and an austenitic phase (γ phase) with 82.8% volume fraction. Content of chromium is 20.56 mass%. γ-phase grains precipitate in α-phase matrix grains. Figure 5 shows the elastic-mapping image together with a line trace of the resonance frequency. Within this image, the resonance frequency changed about 0.06%, which is much larger than the accuracy of the resonance-frequency measurement (∼ 0.0001%). The linear trace of the resonance frequency shows that the α-phase modulus is larger than the γ-phase modulus in the region between 220-930 μm, but this relationship is reversed outside this region. Our view of this observation is as follows. The orientation of the γ-phase grain is determined by that of the α-phase grain before precipitation. Precipitation occurs so as to cause minimum elastic-strain energy due to lattice misfit and there should be specific orientation relationships between the α and γ grains. Thus, γ-phase grains with similar resonance frequencies were precipitated in the same α-phase grain. Vertical broken lines in Fig. 5 indicate possible grain boundaries in the α phase.

The second material tested was a superconducting wire consisting of an oxygen-free copper matrix and embedded NbTi filaments of 32 μm diameter.[17,18] Figure 6 shows the cross sections observed by optical microscopy, resonance-ultrasound microscopy, and a line trace of the frequency. The direction-over-averaged Young's moduli of copper and NbTi are 128.7 GPa[17] and 84.3 GPa,[19] respectively. Thus, the resonance frequency on copper is larger than that on NbTi, being consistent with our results. We compare the measured resonance-frequency shift with that calculated using the static Hertzian-contact model in Fig. 7. The scatterings of measured frequencies are caused by different grain orientations: Young's modulus of copper can vary between 66.7 GPa and 190.8 GPa depending on the grain orientation because of its high anisotropy. Also, Young's modulus of NbTi (bcc. phase at room temperature) varies between

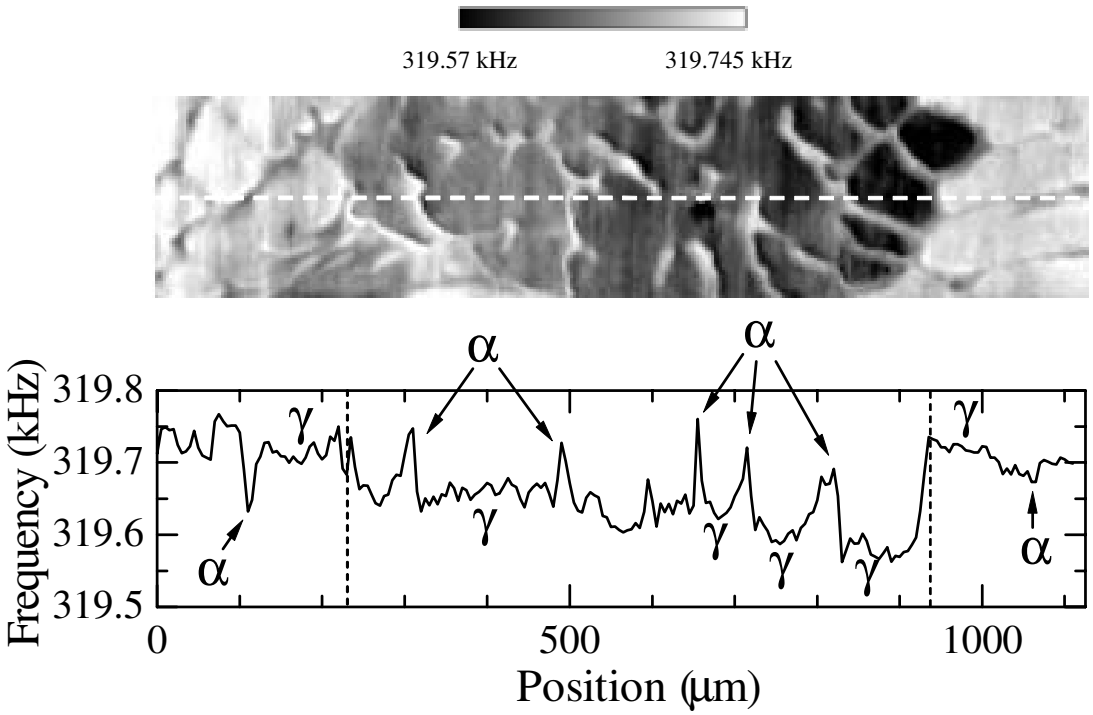

Fig. 5. Resonance-frequency image (top side) and the change in the resonance frequency along the white broken line in the image (lower side) observed for a duplex stainless steel (JIS-SCS13A). Vertical broken lines indicate grain boundaries of α phase.

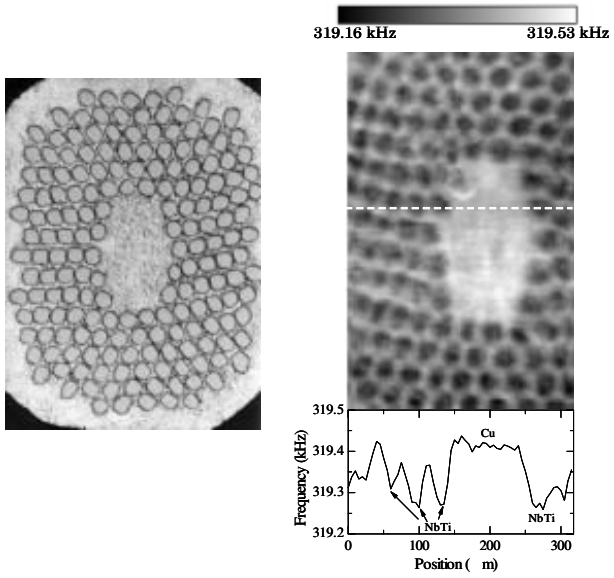

Fig. 6. Microstructure of a NbTi/Cu superconducting wire observed by optical microscopy (left) and resonant-ultrasound microscopy RUM (right). The change in the resonance frequency along the white broken line is also shown.

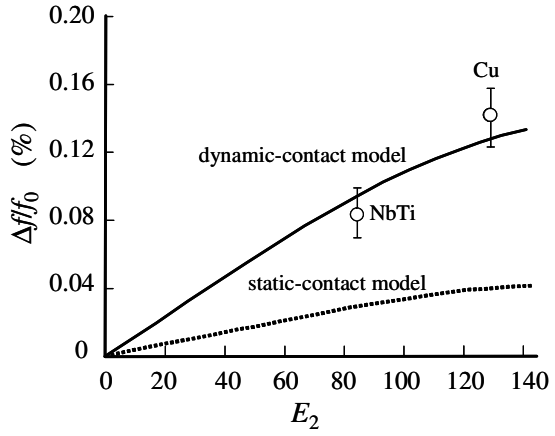

Fig. 7. Resonance-frequency shift versus Young's modulus of contact material. Broken and solid curves are results predicted with the static and dynamic contact stiffnesses, respectively. Solid circles denote measured values.

63.6 GPa and 107.6 GPa. The static contact-stiffness model obviously underestimates the frequency shift by a factor of 3-4, although the trend agrees with the measured values.

We attribute this disagreement to omission of the dynamic effect. The static Hertzian-contact model assumes a flat contact interface, but the actual interface shows curvature. It also neglects the mass density and viscosity of the specimen. However, the contact interface vibrates with the langasite crystal at high frequencies and the contact stiffness should be affected by the mass density and viscosity of the specimen. In particular, the inertia resistance of the specimen should increase the dynamic contact stiffness. The analytical approach for calculating the dynamic contact stiffness including the nonflat contact interface is possible by applying an elastic-wave field in the specimen, which is launched at the contact area by the oscillator, to the boundary condition of the oscillator's oscillation. Indeed, our previous study predicts

that the contact stiffness increases by a factor 2.4 for an isotropic sphere oscillator.[20] Thus, it is predicted that the dynamic contact stiffness is usually larger than the static contact stiffness. The dynamic contact stiffness for a nonspherical oscillator is unavailable theoretically and a numerical approach is needed, which will be the focus of our future work. Here, we roughly estimated the ratio between the static and dynamic stiffnesses to be 3.3 for the present oscillator by comparing the measured and calculated values as shown in Fig. 7.

5. Conclusion

We developed one-point-contact resonance-ultrasound microscopy for evaluating Young's modulus in a local surface region of solids. The vibration of the langasite crystal is isolated using noncont excitation and detection through a quasi-static electric field. The A_g-1 mode showed the highest sensitivity to the material's Young's modulus. The measured frequency shifts were larger than those predicted by the static contact-stiffness model based on the Hertzian contact and the necessity of including consideration of the dynamic contact stiffness is suggested. RUM yielded elastic mappings on a duplex stainless steel and a NbTi/Cu superconducting wire.

Acknowledgment

This study was supported by Industrial Technology Research Grant Program in 2004 from the New Energy and Industrial Technology Development Organization (NEDO).

1) K. Yamanaka, H. Ogiso and O. Kolosov: Appl. Phys. Lett. **64** (1994) 178.
2) O. Wright and N. Nishiguchi: Appl. Phys. Lett. **71** (1997) 626.
3) U. Rabe, J. Turner and W. Arnold: Appl. Phys. A **66** (1998) S277.
4) K. Yamanaka and S. Nakano: Jpn. J. Appl. Phys. **35** (1996) 3787.
5) K. Yamanaka, T. Tsuji, A. Noguchi, T. Koike and T. Mihara: Rev. Sci. Inst. **71** (2000) 2403.
6) G. Yaralioglu, F. Degertekin, K. Crozier and C. Quate: J. Appl. Phys. **87** (2000) 7491.
7) A. Bungo, C. Jian, K. Yamaguchi, Y. Sawada, S. Uda and Y. Pisarevsky: Jpn. J. Appl. Phys. **38** (1999) 3239.
8) H. Ogi, N. Nakamura, K. Sato, M. Hirao and S. Uda: IEEE Trans. Ultrason. Freq. Contr. **50** (2003) 553.
9) H. Ogi, J. Tian, T. Tada and M. Hirao: Appl. Phys. Lett. **83** (2003) 464.
10) M. Hirao and H. Ogi: *EMATs for Science and Industry: Noncontacting Ultrasonic Measurements* (Kluwer-Academic, Boston, 2003).
11) H. Ogi, K. Wada and M. Hirao: Jpn. J. Appl. Phys. **43** (2004) 3024.
12) H. Ogi, E. Goda and M. Hirao: Jpn. J. Appl. Phys. **42** (2003) 3020.
13) I. Ohno: Phys. Chem. Minerals **17** (1990) 371.
14) H. Ogi, Y. Kawasaki, M. Hirao and H. Ledbetter: J. Appl. Phys. **92** (2002) 2451.
15) H. Ogi, M. Fukunaga, M. Hirao and H. Ledbetter: Phys. Rev. B, **69** (2004) 024104.
16) J. Tian, H. Ogi, T. Tada and M. Hirao: J. Acoust. Soc. Am. **115** (2004) 630.
17) H. Ledbetter, J. Moulder and M. Austin: Wire J. **31** (1981) 27.
18) S. Kim, H. Ledbetter and H. Ogi: J. Appl. Phys. **88** (2000) 2378.
19) C. Reid, J. Routbort and R. Manynard: J. Appl. Phys. **44** (1973) 1398.
20) J. Tian, H. Ogi and M. Hirao: J. Appl. Phys. **95** (2004) 8366.